

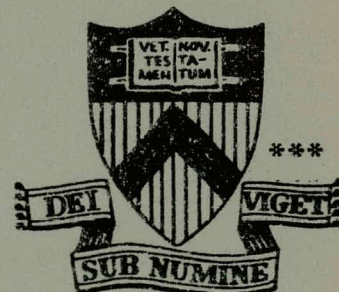
MULTIGROUP CALCULATIONS OF LOW
ENERGY NEUTRAL TRANSPORT IN
TOKAMAK PLASMAS

MASTER

BY

J. G. GILLIGAN, S. L. GRALNICK,
W. G. PRICE, JR., AND T. KAMMASH

**PLASMA PHYSICS
LABORATORY**



DISTRIBUTION OF THIS DOCUMENT IS UNLIMITED

**PRINCETON UNIVERSITY
PRINCETON, NEW JERSEY**

This work was supported by U. S. Energy Research and Development Administration Contract EY-76-C-02-3073. Reproduction, translation, publication, use and disposal, in whole or in part, by or for the United States Government is permitted.

DISCLAIMER

This report was prepared as an account of work sponsored by an agency of the United States Government. Neither the United States Government nor any agency Thereof, nor any of their employees, makes any warranty, express or implied, or assumes any legal liability or responsibility for the accuracy, completeness, or usefulness of any information, apparatus, product, or process disclosed, or represents that its use would not infringe privately owned rights. Reference herein to any specific commercial product, process, or service by trade name, trademark, manufacturer, or otherwise does not necessarily constitute or imply its endorsement, recommendation, or favoring by the United States Government or any agency thereof. The views and opinions of authors expressed herein do not necessarily state or reflect those of the United States Government or any agency thereof.

DISCLAIMER

Portions of this document may be illegible in electronic image products. Images are produced from the best available original document.

NOTICE

This report was prepared as an account of work sponsored by the United States Government. Neither the United States nor the United States Energy Research and Development Administration, nor any of their employees, nor any of their contractors, subcontractors, or their employees, makes any warranty, express or implied, or assumes any legal liability or responsibility for the accuracy, completeness or usefulness of any information, apparatus, product or process disclosed, or represents that its use would not infringe privately owned rights.

Printed in the United States of America.

Available from
National Technical Information Service
U. S. Department of Commerce
5285 Port Royal Road
Springfield, Virginia 22151
Price: Printed Copy \$ * ; Microfiche \$3.00

<u>*Pages</u>	<u>NTIS Selling Price</u>
1-50	\$ 4.00
51-150	5.45
151-325	7.60
326-500	10.60
501-1000	13.60

MULTIGROUP CALCULATIONS OF LOW ENERGY NEUTRAL
TRANSPORT IN TOKAMAK PLASMAS

J. G. Gilligan, S. L. Gralnick, W. G. Price, Jr.,
Princeton University, Plasma Physics Laboratory
Princeton, New Jersey 08540

and


T. Kammash

University of Michigan, Dept. of Nuclear Engineering
Ann Arbor, Michigan

PPPL-1384

September 1977

NOTICE
This report was prepared as an account of work sponsored by the United States Government. Neither the United States nor the United States Energy Research and Development Administration, nor any of their employees, nor any of their contractors, subcontractors, or their employees, makes any warranty, express or implied, or assumes any legal liability or responsibility for the accuracy, completeness or usefulness of any information, apparatus, product or process disclosed, or represents that its use would not infringe privately owned rights.

DISTRIBUTION OF THIS DOCUMENT IS UNLIMITED 

MULTIGROUP CALCULATIONS OF LOW ENERGY NEUTRAL
TRANSPORT IN TOKAMAK PLASMAS

J. G. Gilligan, S. L. Gralnick, W. G. Price, Jr.,
Princeton University, Plasma Physics Laboratory
Princeton, New Jersey 08540

and

T. Kammash

University of Michigan, Dept. of Nuclear Engineering
Ann Arbor, Michigan

PPPL-1384

September 1977

MULTIGROUP CALCULATIONS OF LOW ENERGY NEUTRAL TRANSPORT
IN TOKAMAK PLASMAS*

J. G. GILLIGAN, S. L. GRALNICK, W. G. PRICE, JR.

Princeton University, Plasma Physics Laboratory

Princeton, N. J.

and

T. KAMMASH

University of Michigan, Dept. of Nuclear Engineering

Ann Arbor, Michigan

ABSTRACT

Multigroup discrete ordinates methods avoid many of the approximations that have been used in previous neutral transport analyses. Of particular interest are the neutral profiles generated as an integral part of larger plasma system simulation codes. To determine the appropriateness of utilizing a particular multigroup code, ANISN, for this purpose, results are compared with the neutral transport module of the Düchs code. For a typical TFTR plasma, predicted neutral densities differ by a maximum factor of three on axis and outfluxes at the plasma boundary by 40%. This is found to be significant for a neutral transport module. Possible sources of the observed discrepancies are indicated from an analysis of the approximations used in the Düchs model. Recommendations are made concerning the future application of the multigroup method.

*This is a preprint of an article to appear in NUCLEAR FUSION.

1. INTRODUCTION

Neutral particles play an important role in the evolution of tokamak plasmas: The recycling of neutrals at the plasma-wall interface regulates the steady state plasma density profile, wall-evolved impurities resulting from neutral sputtering can seriously effect plasma resistivity, confinement times and radiation loss rates, escaping charge exchange neutrals can substantially cool the peripheral plasma regions, and the coupling of high energy neutral beams into the plasma is greatly reduced by the presence of the background neutral population.

The accurate prediction of neutral atom profiles is essential, but many previously used techniques are restricted in their range of applicability. We will demonstrate that multigroup discrete ordinates methods allow a more rigorous analysis than has customarily been employed in neutral computational procedures. Fewer approximations and simplifications are required in treating the transport problem.

Of primary importance are neutral distributions generated repeatedly for utilization in larger plasma simulation codes. To determine the practicality of using multigroup methods for this purpose we compare our results to those of the neutral transport module of the Düchs code [1]. Given the increased rigor of the multigroup method, it can be used as a check on the accuracy of the Düchs treatment. The

discrepancies are examined to determine their significance in the computational modeling of tokamak systems. The results of the comparison study lead us to recommend areas where multigroup discrete ordinates methods will be of significant value.

Section 2 constitutes a review of previous neutral calculational techniques with an emphasis on the approximations and simplifications that have gone into each. We treat the Duchs model in special detail since it will later serve as the comparison case. Multigroup discrete ordinates methods are also briefly described along with their application to neutral transport up to this time. The neutral-plasma interaction model we use is given in Section 3. The results of the comparison study are presented in Section 4.

2. REVIEW OF NEUTRAL CALCULATIONAL PROCEDURES.

2.1. Previous Methods

We begin our discussion with the integro-differential (Eq. 1) and integral (Eq. 2) forms of the linear Boltzmann transport equation [2].

$$\underline{\Omega} \cdot \nabla \phi + \sigma_a(\underline{r}, E) \phi(\underline{r}, \underline{\Omega}, E) = q(\underline{r}, \underline{\Omega}, E) + Q(\underline{r}, \underline{\Omega}, E) \quad (1)$$

$$\Phi(\underline{r}, \underline{\Omega}, E) = \int_0^{\infty} \exp \left[- \int_0^{s'} \sigma_a(\underline{r}-\underline{s}'', \underline{\Omega}, E) ds'' \right] \times \left(q(\underline{r}-\underline{s}', \underline{\Omega}, \underline{\Omega}, E) + Q(\underline{r}-\underline{s}', \underline{\Omega}, \underline{\Omega}, E) \right) ds' \quad (2)$$

where $\Phi(\underline{r}, \underline{\Omega}, E)$ is the angular neutral flux, $\sigma_a(\underline{r}, E)$ is the total absorption cross section, $q(\underline{r}, \underline{\Omega}, E)$ is the effective scattering source due to charge exchange and $Q(\underline{r}, \underline{\Omega}, E)$ is the stationary neutral source. In neutral transport problems the absorption cross section and scattering source are given by,

$$\begin{aligned} \sigma_a(\underline{r}, E) &= \frac{1}{v} \int_{E', \underline{\Omega}'} N_i(\underline{r}) h_i(\underline{r}, E') |\underline{v}-\underline{v}'| \sigma_{ii}(|\underline{v}-\underline{v}'|) \frac{dE' d\underline{\Omega}'}{4\pi} \\ &+ \frac{1}{v} \int_{E', \underline{\Omega}'} N_e(\underline{r}) h_e(\underline{r}, E') |\underline{v}-\underline{v}'| \sigma_{ei}(|\underline{v}-\underline{v}'|) \frac{dE' d\underline{\Omega}'}{4\pi} \\ &+ \frac{1}{v} \int_{E', \underline{\Omega}'} N_i(\underline{r}) h_i(\underline{r}, E') |\underline{v}-\underline{v}'| \sigma_{cx}(|\underline{v}-\underline{v}'|) \frac{dE' d\underline{\Omega}'}{4\pi} \end{aligned} \quad (3)$$

and

$$q(\underline{r}, \underline{\Omega}, E) = N_i(\underline{r}) \frac{h_i(\underline{r}, E)}{4\pi} \int_{E', \underline{\Omega}'} \Phi(\underline{r}, \underline{\Omega}', E') \frac{1}{v} |\underline{v}-\underline{v}'| \sigma_{cx}(|\underline{v}-\underline{v}'|) dE' d\underline{\Omega}' \quad (4)$$

In equation (3), v is the neutral particle velocity ($v = \sqrt{\frac{2E}{m_n}}$ where m_n is the neutral mass), $N_i(N_e)$ is the ion (electron) density and $h_i(h_e)$ is the ion (electron) distribution function. The target velocity v' is calculated as $v' = \sqrt{\frac{2E'}{m_{i,e}}}$ where the mass, $m_{i,e}$, refers to either ions or electrons. The microscopic cross sections σ_{ii} , σ_{ei} , and σ_{cx} represent ion

impact ionization, electron impact ionization and charge exchange reactions respectively. We have assumed that h_i and h_e are isotropic and are normalized so that

$$\int_0^{\infty} h_{i,e}(E) dE = 1 \quad (5)$$

Equations (1) and (2) are equivalent descriptions of the transport process and both have been used as starting points for the calculation of neutral atom distributions in tokamak plasmas. To arrive at mathematically tractable solutions, however, a number of simplifying assumptions have been employed. The early work of Zubarev and Klimov [3] considers a one-dimensional model and assumes that the neutral energy distribution is a Maxwellian at the ion temperature. Dnestrovskii, Kostomarov and Pavlova [4] retain the slab model but do not make a priori assumptions about the neutral flux distribution. This approach leads to an integral equation (in the angular flux $\Phi(r, \underline{\Omega}, E)$) of the form of equation (2). The ion distribution function is chosen so that a charge exchange neutral has an energy equal to the local ion temperature and is scattered into one of two directions, forward or back. That is,

$$h_i = \delta(v+v_i) + \delta(v-v_i) \quad (6)$$

where v_i is the local ion thermal velocity. An approximation for the charge exchange cross section is also introduced so that,

$$|\underline{v}-\underline{v}'| \sigma_{\text{cx}}(|\underline{v}-\underline{v}'|) = C \quad (7)$$

where C is a constant ($\text{cm}^3 \text{sec}^{-1}$) determined by the local ion temperature. When equation (7) is substituted into equation (4), the angular dependence (on $\underline{\Omega}$) is removed from the expression for q . This also allows $\underline{\Omega}$ to be integrated out of equation (2), with the the resulting integral equation a function of the scalar flux $\phi(\underline{r}, E)$. In reality the product on the left hand side of equation (7) increases as a function of the relative energy (shown in Fig. 1) but not so much as to invalidate the approximation in the regime of interest ($< 10 \text{ keV}$). Rehker and Wobig [5] use a similar analysis with an approximation for the charge exchange cross section also given by equation (7). However, the plasma ions are assigned a more realistic Maxwellian distribution function. Only homogeneous plasmas are considered. Hogan and Clarke [6] treat realistic plasma temperature and density profiles in slab geometry. An approximation for the charge exchange cross section similar to equation (7) is also employed. Later, Clarke and Sigmar [7] investigate the effect of reflected outfluxed neutrals at the plasma boundary but restrict themselves to a homogeneous plasma in

planar geometry. The ion distribution function is approximated by a finite temperature "Maxwellian" and has the form

$$h_i = \delta(v - \alpha_i) (1 + 3v_x u_i / \alpha_i^2) (1/4\pi v^2) \quad (8)$$

α_i = Ion thermal velocity

u_i = Toroidal flow velocity

The charge exchange cross section is assumed to behave as in reference [6].

For high neutral-plasma collisional regimes some computational techniques (the Düchs treatment in particular) have proved to have poor convergence properties (discussed later in this section). In an attempt to circumvent the problem Molvig [8] uses a Fourier transformation method to arrive at neutral density profiles. The integro-differential transport equation with the convenient approximation for the charge exchange cross section (equation 7) is used. The solutions are obtained in infinite cylindrical (one-dimensional) geometry which presumably will model the actual toroidal configuration more closely than the slab approximation. Molvig's analysis also assumes the plasma to be radially uniform in temperature, but a density profile is allowed.

To examine the interaction of a neutral gas blanket with a plasma, Lehnert uses a set of macroscopic fluid equations [9]. The assumption here is that $\lambda_n \ll L$ where λ_n is the neutral attenuation length and L is a characteristic

dimension of the system. For a homogeneous plasma in slab geometry a neutral attenuation length can be derived that is a function of the plasma properties and the neutral-plasma reaction rates.

The Dúchs [1] treatment is based upon the integral form of the transport equation. An iterative solution technique for the neutral density leads to the identification of the resulting series as representing "generations" of charge exchange neutrals. (We therefore refer to the Dúchs neutral treatment as the generation method.) We see this by substituting equation (4) into equation (2) with the following series generated for the flux:

$$\phi = \sum_{i=1}^n L^i \phi^0 + \phi^0 \quad (9)$$

where L is the integral transport operator and ϕ^0 is the uncollided neutral flux. The sum of the terms in equation (9) represent the solution, provided the series converges. The presence of ionization (absorption) of neutrals guarantees this [5,8] since the effective expansion parameter of the series, β , is given as

$$\beta = \frac{\langle \sigma v \rangle_{cx}}{\langle \sigma v \rangle_{cx} + \langle \sigma v \rangle_{ei}} < 1 \quad (10)$$

where $\langle\sigma v\rangle_{cx}$ and $\langle\sigma v\rangle_{ei}$ are average reaction rates for charge exchange and electron impact ionization. What is not known though, is the number of terms required for an accurate solution, since β does not solely gauge the relative size of the terms in the series [8]. If the optical depth of the plasma is defined as

$$\rho = \int_0^a dr' \left(\frac{N_i \langle\sigma v\rangle_{cx}}{v_n} + \frac{N_e \langle\sigma v\rangle_{ei}}{v_n} \right), \quad (11)$$

where a is the minor radius and v_n is a characteristic neutral velocity, then for plasmas with $\rho \gg 1$, many more terms are required in the series solution to account for the high collisionality. Ten generations of charge exchange neutrals are used in present codes but it has been pointed out that this may not be adequate for higher density plasmas [1,8].

Since not all of the assumptions used in the generation method are stated explicitly in Reference [1] we give a derivation of the approximate integral transport equation in the Appendix. Specific reference to these assumptions (which are summarized below) is made in Section 4 where the discrepancies between the two methods in the comparison study are traced.

As seen in the Appendix the generation method assumes the charge exchange source to be a function of the density $n^g(\underline{r}, E')$ rather than the angular density $n^g(\underline{r}, \underline{\Omega}', E')$. The $\underline{\Omega}$ dependence of the source term is thus removed which greatly

simplifies the computational solution. The effect of this isotropic approximation is explored by the multigroup method and discussed in Section 4. Regarding the energy variable, the ion distribution function is assumed to be $\delta(E-kT_i)$, and thus monoenergetic at the local kT_i . The energy distribution of the current neutral generation ($n^g(E)$) is also assumed monoenergetic at a kT^g . The "temperature", kT^g , is obtained as an average over the temperatures of the neutrals that reach the space point in question. The modal treatment of the energy variable is convenient but implies that the character of all aspects of energy transfer can be approximated with averaged Maxwellian parameters. Finally, the exponential function is used as an approximation to the function Ki_1^* as the integral attenuation term. The latter function is arrived by integrating out the angular coordinate corresponding to the z axis in infinite cylindrical geometry. This approximation (transport in a disk) is seen to be valid for only a small range of the attenuation parameter ρ (seen in Fig. A.2).

2.2. Multigroup Discrete Ordinates Methods

The feasibility of using multigroup discrete ordinates methods for neutral transport was first pointed out by Greenspan [11]. The first applications involved an approximation which simplified the energy treatment [11] and a pure attenuation problem [12]. Since then several authors have explored neutral transport in ORMAK [13] and EPR type

*The first repeated integral of the Bessel Function.

devices [14] with an emphasis on the practical application of the method. Marable and Oblow [13] additionally examined the effect of the boundary condition for outfluxed neutrals.

The multigroup discrete ordinates method [2,15,16] of solving the Boltzmann transport equation (differential form) is based on the discretization of all the independent variables; space \underline{r} , direction $\underline{\Omega}$, and energy E . Differentials are approximated by finite differences and integrals by weighted sums to yield a set of coupled (in energy and angle) algebraic equations suitable for an iterative solution on the computer. This widely used and highly successful class of transport equation solvers was designed to yield accurate results for deep neutron penetration problems even where pronounced anisotropic scattering and energy dependent cross sections were encountered. In principle the only limit on accuracy is the size and speed of the computer which restricts the fineness of the space, angle and energy meshes.

A feature of many multigroup discrete ordinates methods is the ability to treat the anisotropic nature of the scattering kernel. The usual procedure is to expand the scattering kernel in a series of Legendre polynomials (P_ℓ) of the relative scattering angle ($\mu_0 = \underline{\Omega} \cdot \underline{\Omega}'$). The truncation of the series after only a few L terms (the P_L scattering approximation) has proved to be adequate even for highly anisotropic scattering.^[16] The charge exchange kernel $(\frac{N_i h_i}{v'} | \underline{v} - \underline{v}' | \sigma_{cx}(|\underline{v} - \underline{v}'|))$ is anisotropic in the sense

that the product $|\underline{v} - \underline{v}'| \sigma_{cx} (|\underline{v} - \underline{v}'|)$ depends upon the relative orientation of the initial and final neutral velocity vectors \underline{v} and \underline{v}' . For example, when $v \sim v'$, collisions which are head on occur at a greater frequency than those for which \underline{v} and \underline{v}' are in the same direction. The situation is reversed for relative energies greater than about 10 keV because the charge exchange cross section drops off much quicker than $1/|\underline{v} - \underline{v}'|$.

The multigroup treatment of the energy variable involves the integration of the Boltzmann equation (equation (1) with the P_L scattering approximation) over the range $E_{g+1} \leq E \leq E_g$, defining the group "g". Multigroup cross sections are defined which are of the form,

$$\sigma_a^g(\underline{r}, \underline{\Omega}) = \int_{E_{g+1}}^{E_g} \sigma_a(\underline{r}, E) \phi(\underline{r}, \underline{\Omega}, E) dE / \phi^g(\underline{r}, \underline{\Omega}) \quad (12)$$

and

$$\sigma_\ell^{h \rightarrow g}(\underline{r}, \underline{\Omega}) = \frac{\int_{E_{h+1}}^{E_h} \phi_\ell(\underline{r}, \underline{\Omega}, E') dE' \int_{E_{g+1}}^{E_g} \sigma_\ell(\underline{r}, E' \rightarrow E) dE}{\int_{E_{h+1}}^{E_h} \phi_\ell(\underline{r}, \underline{\Omega}, E') dE'} \quad (13)$$

where ϕ_ℓ and σ_ℓ are Legendre expansion coefficients for the angular flux ϕ and the scattering kernel respectively. In principle the general multigroup formulation is an exact treatment of the energy variable provided the weighting functions ϕ_ℓ and ϕ are known exactly. This is of course not possible, but a good solution can still be obtained if a

sufficient number of groups, appropriately structured, are used to make up for the uncertainty that a poor weighting function might introduce. Better values for the weighting functions (with the possibility of requiring fewer groups) can be obtained in an iterative manner.

The essential basis of discrete ordinates methods is that the angular distribution of the particle flux is evaluated in a number of discrete directions. By considering enough directions an arbitrarily accurate evaluation of the angular flux can be obtained. Care is taken to include rays in all directions for a particular geometry (e.g. down the axis in infinite cylindrical geometry).

To summarize: Multigroup discrete ordinates methods are able to treat the energy, angular and spatial dependences which have only been approximated by other neutral analysis techniques. These approximations have been demonstrated explicitly for the case of the "generation" method. We refer specifically to the assumptions of isotropic charge exchange source, the monoenergetic source of charge exchange neutrals (at kT_i), the ensuing averaging to obtain the neutral spectrum, and the restriction to transport in a planar disk.

3. NEUTRAL-PLASMA MODEL

Of the many possible interactions which can occur between neutral hydrogen atoms and a tokamak plasma only a

few have a substantial effect on the neutral transport. These are charge exchange, electron impact ionization and ion impact ionization. Although the cross section for an elastic collision between a proton and a hydrogen neutral is of the same order of magnitude as that for charge exchange, very little momentum is transferred in the former process. Hence the trajectory of the neutral remains nearly unchanged, and the collision may be ignored. Likewise the temperature regime of interest ($T_e > 1$ eV) permits volumetric recombination of ions and electrons (to the neutral state) to be neglected as a source of neutrals. Convenient analytical fits for ionization and charge exchange cross sections are obtained from Riviere [17] for use in the multigroup expressions (equations (12) and (13)).

The physical model we consider assumes hydrogen atoms incident on a proton and electron plasma ($N_e = N_i$) in an infinitely long cylinder. The calculations are performed in cylindrical coordinates. The plasma temperature and density are specified on a set of concentric shells each characterized by an isotropic Maxwellian distribution function ($T_e = T_i$); the plasma properties are homogeneous in each shell. Throughout the calculation it is assumed that the plasma profiles remain fixed as the neutrals relax to the steady state.

It has been demonstrated that a critical part of the neutral calculation depends upon the modeling of the source neutrals and the boundary condition chosen for the

outfluxed* neutrals [7]. For the purposes of the comparison study, desorbed hydrogen gas (H_2) from the outer material wall is assumed to immediately undergo dissociative ionization, forming Franck-Condon neutrals with energies of about 3 eV. In reality the disassociation process takes place over a finite volume, frequently small in comparison to the plasma dimensions; this effect will be neglected here. The resulting inward neutral current at the boundary is assumed to originate from an isotropic monoenergetic flux distribution (at an energy of 3 eV). The results of the study are scaled to a neutral edge density equivalent to this flux value.

Outfluxed neutrals can either be absorbed or reflected (perhaps with some energy degradation) at the boundary. Few data exist in this area, but Robinson's calculations for hydrogen atoms bombarding polycrystalline copper indicate that the reflection coefficient is about .2 at an incident energy of 3 keV [18]. The corresponding energy reflection coefficient is .09. The effect of reflected neutrals is to extend the overall penetration into the plasma with a corresponding increase in neutral density. Here we assume that all outfluxed neutrals stick to the outer material boundary (absorption coefficient of unity)

*The term "outflux" actually refers to the outward current ($cm^{-2} sec^{-1}$) of neutrals (primarily due to charge exchange) at the outer plasma boundary.

and we neglect the possibility that additional adsorbed molecules will be dislodged from the surface by the outflux.

As a basis for comparison two test cases are chosen. Shown in Fig. 2(a) and (b) are "snapshot" plasma profiles of the ST [19] and TFTR [20] tokamaks. The profiles are of the form

$$\begin{aligned} T &= T_0 \left(1 - \left(\frac{r}{r_0} \right)^\alpha \right) + T_B \\ N &= N_0 \left(1 - \left(\frac{r}{r_0} \right)^\beta \right) + N_B \end{aligned} \tag{14}$$

with the constants (displayed in Table I.) chosen to typify experimental and design data for the ST and TFTR machines respectively. The choices are made to determine if the effects of plasma temperature, density and size will modify the relative performance of the two methods. A good indication of the difference in quality of the plasma is given by the parameter ρ (the number of neutral collision mean free paths in the plasma, defined in Section 2). For ST we calculate (using average values) $\rho \sim .8$ while for TFTR $\rho \sim 3$.

4. COMPARISON STUDY RESULTS

A code, GIMUXS [29], was written to generate multigroup cross section libraries (using equations of the

form (12) and (13)) suitable for use with the one-dimensional, multigroup, discrete ordinates, transport code ANISN [21]. Up to P_3 scattering order cross sections can be calculated by GIMUXS; variable temperature, Maxwellian target distribution functions, and arbitrary energy group structures can also be considered.

Several approximations aid in the evaluation of equations (12) and (13). We have assumed that the cross section weighting function ($\Phi(\underline{r}, \underline{\Omega}, E)$ and $\phi_\ell(\underline{r}, \underline{\Omega}, E)$) can be written as a product of functions (separation of variables) of the form

$$\Phi(\underline{r}, \underline{\Omega}, E) = \Phi(\underline{r}, \underline{\Omega}) f(E) \tag{15}$$

$$\phi_\ell(\underline{r}, \underline{\Omega}, E) = \phi_\ell(\underline{r}, \underline{\Omega}) f_\ell(E)$$

The functions $f(E)$ and $f_\ell(E)$ are further assumed to be piecewise constant within each energy group. Using equations (15), the integration in the denominator of equations (12) and (13) can be performed to yield

$$\sigma_a^g(\underline{r}, E) = \frac{1}{E_g - E_{g+1}} \int_{E_{g+1}}^{E_g} \sigma_a(\underline{r}, E) dE \tag{16}$$

$$\sigma_\ell^{h \rightarrow g}(\underline{r}, E) = \frac{1}{E_h - E_{h+1}} \int_{E_{h+1}}^{E_h} \int_{E_{g+1}}^{E_g} \sigma_\ell(\underline{r}; E' \rightarrow E) dE dE'$$

From an examination of equations (3) and (4) the expressions for σ_a and σ_ℓ can be decomposed as

$$\sigma_a(\underline{r}, E) = \langle \sigma v \rangle \frac{N(\underline{r})}{v} \quad (17)$$

$$\sigma_\ell(\underline{r}, E' \rightarrow E) = \langle \sigma v \rangle_\ell N(\underline{r}) \frac{h_i(E)}{4\pi} \frac{1}{v'}$$

where

$\langle \sigma v \rangle$ = the total reaction rate ($\text{cm}^3 \text{sec}^{-1}$) of a neutral particle of energy E with a plasma,

and

$$\langle \sigma v \rangle_\ell = 2\pi(2\ell + 1) \int_{-1}^1 |\underline{v} - \underline{v}'| \sigma_{cx}(|\underline{v} - \underline{v}'|) P_\ell(\mu_0) d\mu_0$$

From experience in generating equation (17) it has been noted that for plasmas where $20 \text{ eV} < T < 20 \text{ keV}$ then $\langle \sigma v \rangle$ is a slowly varying function of E and $\langle \sigma v \rangle_\ell$ is a slowly varying function of E and E' for contributions from significant ℓ values. It is maintained that a suitable group structure can be chosen (discussed below) so that $\langle \sigma v \rangle$ and $\langle \sigma v \rangle_\ell$ can be considered constants within each group so that when equations (17) are substituted into equation (16) then

$$\sigma_a^g(\underline{r}, E) = \frac{N(\underline{r})}{E_g - E_{g+1}} \langle \sigma v \rangle (\bar{E}_g) \int_{E_{g+1}}^{E_g} \frac{1}{v} dE$$

$$\sigma_\ell^{h \rightarrow g}(\underline{r}, E) = \frac{N(\underline{r})}{E_h - E_{h+1}} \langle \sigma v \rangle_\ell (\bar{E}_g, \bar{E}_h) \int_{E_{g+1}}^{E_g} \frac{h_i(E)}{4\pi} dE \int_{E_{h+1}}^{E_h} \frac{1}{v'} dE'$$

(18)

where $\bar{E}_g = \frac{E_g + E_{g+1}}{2}$. The remaining integrals can be performed analytically to yield

$$\sigma_a^g(\underline{r}, E_g) = N(\underline{r}) \langle \sigma v \rangle (\bar{E}_g) S(E_g) \quad (19)$$

$$\sigma_\ell^{h \rightarrow g}(\underline{r}, E_g, E_h) = N(\underline{r}) H_i(\underline{r}) \langle \sigma v \rangle_\ell(\bar{E}_g, \bar{E}_h) S(E_g) ,$$

where

$$S(E_g) = \frac{2}{B(\sqrt{E_g} + \sqrt{E_{g+1}})}$$

$$B = 1.39 \times 10^6 \text{ cm sec}^{-1} \text{ eV}^{-1/2}$$

$$H_i(E_g) = \int_{E_{g+1}}^{E_g} \frac{h_i(E)}{4\pi} dE .$$

The original three-dimensional iterated integrals (equations (12) and (13)) have been reduced to a product of one-dimensional integrals with a corresponding decrease in computation time. The effects of the approximations will be minimal and mitigated by the choice of a finer energy group mesh.

Several considerations are taken into account for the selection of an energy group structure. These are: resolution of the expected energy spectra, consistency with

the cross section approximations introduced, and efficiency of the transport equation solver. It is known that after several charge exchange events the neutral population will take on the characteristics of the target ions (below $E \sim 20$ keV). These will be Maxwellian energy distributions ranging from low temperatures ($T \sim 20$ eV) at the plasma edge to high temperatures at the plasma core ($T \sim 10$ keV). The tendency for Maxwellian distributions to be more skewed for low temperatures and the need to cover a wide range in energy suggests that the energy groups be narrower in the low energy regime and wider as energy is increased. For this purpose equal increments in $\log E$ are sufficient.

It is recalled that the variation of $\langle \sigma v \rangle$ and $\langle \sigma v \rangle_\ell$ with energy was noted to be mild. The behavior is smooth enough to suggest that a group structure with equal logarithmic increments will also be adequate to satisfy the approximation criteria: namely that $\langle \sigma v \rangle$ and $\langle \sigma v \rangle_\ell$ are constant within each group.

For the multigroup codes it is advantageous to arrange the energy group structure so that the particle flux is distributed evenly between groups. Since the neutral flux will be approximately Maxwellian in the volume of the plasma an estimate can be made of the amount of flux as a function of an energy interval. The total fraction of particles in a Maxwellian flux distribution up to an energy ϵ is given by A , where

$$A = \int_0^x \left(\frac{E}{T}\right) \exp\left(-\frac{E}{T}\right) d\left(\frac{E}{T}\right)$$
$$= 1 - e^{-x} (x + 1)$$

where $x = \frac{\epsilon}{T}$.

A is plotted as a function x in Fig. 3. The abscissa has a logarithmic scale and it is seen that for the range $.6 < x < 5$, A is approximately linear in $\log x$ (compare to the dashed line). The particles in this range represent about 80% of those in the entire distribution. In the linear region then, energy groups formed by equal increments in $\log \frac{\epsilon}{T}$ will contain approximately equal fractions of the particle flux.

For the reasons considered above an energy structure which is based on a uniform mesh in $\log E$ is chosen. The intervals span the range 0-55 keV, which will contain most of the particles in Maxwellian distributions with temperatures less than 10 keV. Shown in Table II are the results of increasing the number of groups for a particular problem. The 31 group structure was felt to be adequate and is used for the remainder of the study.

An interesting feature we present is the use of reverse labelling for the group structure, as opposed to the conventional (neutron analysis) designation that gives the highest energy the label "1". In neutron transport the predominant energy transition

is downscatter, and the multigroup codes make use of this fact in sweeping from high to low energy groups to maximize the efficiency. The transport of edge source neutral atoms into a plasma on the other hand is dominated by upscattering (i.e. charge exchange with more energetic plasma ions), and therefore the advantage is lost. If the group labeling is reversed, however, scattering is once more from low to high group number, and a savings in iteration time of as much as 50% can be realized. [29]

A summary of the operating parameters of both the multigroup method (ANISN) and the neutral transport procedure of the Düchs code is given in Tables III and IV. We use the isotropic (P_0) scattering approximation for the charge exchange source term and an S_8 angular quadrature in making the ANISN runs. The choice of a P_0 expansion is based on the results of a comparison with P_1 and P_3 transport in a plasma similar to that of the TFTR machine. The total relative attenuation of the neutral density and the average energy of the neutral outflux are displayed in Table V. Little effect is noticed as a higher order scattering approximation is used. The primary reason for this is thought to be that very few charge exchange pairs in a Maxwellian plasma have comparable velocities ($v \sim v'$) which would maximize anisotropy. We conclude that the restriction to isotropic scattering is not serious. Our findings are also consistent with the results of El Derini and Gelbard [14].

Throughout this study we have observed that neutral transport is highly sensitive to plasma conditions near the neutral source (the plasma edge in this case), since the first charge exchange neutrals originate in this region. To eliminate the possibility of discrepancies arising from this effect, the plasma zone (temperature and density) structure used for the ANISN cases was chosen to be the same as that determined by the standard Düchs code. The model we use for incident source neutrals and the boundary conditions for outfluxed neutrals was explained in Section II. We emphasize here that entirely equivalent conditions are utilized by the generation method [1]. The main ingredient in both instances is the specification of the normalizing cold neutral density at the boundary.

Neutral densities as a function of plasma radius are displayed in Fig. 4 for the ST and TFTR machines. The multigroup results are seen to be consistently lower than the generation method, reaching a maximum discrepancy of about a factor of three on the TFTR axis. The ST densities differ by no more than 50%. We have chosen as the normalization a neutral atom edge density of $1 \times 10^{10} \text{ cm}^{-3}$ (equivalent to a neutral gas (H_2) pressure of $\sim 1.5 \times 10^{-7}$ Torr at $T = .025 \text{ eV}$) which is fairly typical of present day discharges. The density in the plasma drops almost immediately to about one half that value, since only $\sim 50\%$ of the isotropic distribution has a velocity component directed into the plasma. Both neutral density profiles are predominantly concave upward. This results from an increase

in ionization. mean free path as the average velocity of the neutrals rises (from charge exchange collisions with more energetic ions) faster than the plasma density increases. Below 100 eV, however, the electron impact ionization rate increases with temperature, reducing the previous trend and explaining the roll over (concave downward) of the neutral density near the ST edge. No such inflection is seen for the TFTR case where the plasma edge is above 200 eV.

The lack of agreement between the two methods can be partially accounted for in at least two ways. The generation method converges poorly for the TFTR case. A significant number of neutrals ($\sim 1/2$ the total on axis) are found to build up in the tenth and final charge exchange generation. The code implementation does not permit these neutrals to charge exchange further [1]. The effect may be to enhance the actual neutral density by shortening the lifetime a neutral may have to undergo ionization in the plasma. For the ST case the plasma was optically thin enough so that only a few charge exchange generations were required to reach a converged solution. It will be recalled (Section 2) that Molvig [8] has pointed out that there may be difficulty in arriving at sufficiently converged solutions for $\rho \gg 1$. The solutions we have seen for TFTR ($\rho \sim 3$) and ST ($\rho \sim .8$) seem to bear this out. The multigroup method exhibits good convergence for all cases considered.

Another factor which may contribute to the observed discrepancies is the exponential approximation to the Ki_1 function employed in the generation method (see Section 2). For $\rho > .7$ the exponential approximation increasingly underestimates the attenuation. This would eventually lead to an overestimate of the neutral density which is consistent with the findings we present here.

A summary of neutral results appear in Table VI where G refers to the generation method and M to multigroup. We see that the outfluxes (currents) of charge exchange neutrals at the boundary differ by as much as 40% while the average energies of the corresponding spectra are in reasonable agreement. That this is so can be seen from plots of the actual spectra in Figs. 5 and 6. We superimpose a Maxwellian flux distribution peaking at about the same energy as that of the spectra to gauge relative shape. The outfluxes are obviously not Maxwellian, exhibiting a lower energy component characteristic of the plasma edge temperature (close to the actual Maxwellians drawn) and a higher energy tail indicative of the ion distribution in the plasma interior. The high energy tail neutrals have been observed experimentally and constitute a means of measuring plasma ion temperatures [22]. The same general spectral shapes have been noted by other authors [6],[23].

The CPU times on an IBM 360/91 for the test cases are displayed in Table VII. The advantage of the generation

method in calculational speed is apparent (by a factor of 20-30). This aspect of neutral module performance is relatively important. For example, for a plasma simulation run by the Düchs code, about 80% of the total run time is devoted to calculating the evolving neutral density. It should be pointed out, however, that the multigroup runs for the comparison study stressed accuracy and consistent modelling and hence "conservative" operating parameters (number of energy groups, space and zone intervals, angular quadratures, etc.) were used.

A parameter survey revealed that a less restrictive operating space drastically reduced computation times while maintaining the advantage of calculational accuracy [29,30]. For example, instead of 99 uniformly spaced plasma temperature zones, 10 zones constructed from the criteria that the approximate neutral interaction mean free path not change by more than a constant between adjacent zones yielded good results. This is shown in the second line of Table VIII. In a like manner, guided by the parameter survey, it was found that S_4 angular quadrature, 28 spatial intervals (with a finer mesh close to the neutral source), a less stringent convergence and 11 energy groups combined to give the results of line 3 of Table VIII. The reduction in the iteration time is seen to be dramatic (by a factor of 75) to a level below that of the standard generation method (line 5). In addition the errors introduced by the relaxed operating parameters are less than ~ 20% but more importantly are less than those of the generation method.

Several supplementary techniques allow further significant time reduction[29,30]. By starting the ANISN iteration procedure with a good initial flux guess fewer iterative cycles are required to reach convergence. In an evolving plasma application, the solution from a previous time step will be available. For restarts from cases where plasma edge temperatures differ by 50% a decrease in execution time by nearly a factor of 2 is possible. Another method that has proved successful is that of limiting the number of ANISN inner iterations. Normally iteration on the self-scatter term requires at most 2-3 passes. The contribution of self-scatter to the total scatter process is minimal, however, and an iteration limit of one has been found to be sufficient. A combination of a restart from a case where plasma temperatures differ by 20% and the inner iteration limit of one are applied to the relaxed operating parameter case to generate the results of line 4 of Table VIII. Virtually no change is seen in the results except for the execution time which has been reduced significantly by a factor of two.

An added consideration for the multigroup execution time is the time necessary to generate the multigroup cross sections. Using the code GIMUXS for the 11 group, 10 zone case this is less than 5 seconds.(IBM 360/91). The majority of this time is used for calculating the ion impact ionization rate (neglected by the generation method) and the electron impact ionization rate (approximated by an

analytical fit in the generation method). Thus even when approximations for the cross sections are not included the total multigroup run time is comparable to that of the generation treatment.

5. IMPLICATIONS

The primary purpose of the generation treatment is to calculate steady state neutral atom profiles as an integral part of a larger plasma simulation code. The neutral calculation is done every few time steps as the plasma distribution evolves. We therefore discuss the significance of the results we have seen with this purpose in mind.

The duration of a present day tokamak discharge is typically several times that of the average particle confinement time. For example, for the ST experiment, particle confinement times reaching a maximum of 13-14 msec were reported for discharges lasting at least 50 msec [19]. Since the plasma density remains roughly constant for a large portion of the discharge, the implication is that the plasma outflux is recycled at the boundary, presumably as "cold" neutral hydrogen. The same recycling behavior is expected to be seen in future machines. In the computer modeling of this process, the rule is usually chosen that the cold neutral influx should match the total particle outflow at the plasma edge. Due to problems in implementing the balance, however, the total number of plasma particles

is not held constant to better than about 10% in a computer run, which is considered adequate [1]. For a typical ST discharge the total particle outflux is divided about equally between charged particles and neutrals [23]. The 30% greater neutral outflux level (see Table VI) predicted by the generation method will therefore overestimate the total particle outflux, by a factor of 15%.

The total outfluxed power carried by neutrals, (shown in Table IX), shows a similar trend. Charge exchange losses in ST are comparable to those of radiation (each about 25% of the total losses) [22]. Therefore the additional 40% neutral power loss given by the generation method represents an increase in total power outflux by about 10%. Experimentally determined typical charge exchange power losses for the ST tokamak are estimated by Hinnoy [23]. If both the generation and multigroup results are scaled separately to neutral source densities which yield his reported outflux level ($2.4 \times 10^{16} \text{ cm}^{-2} \text{ sec}^{-1}$) then Table X is derived. Both methods are seen to agree well with experimental observation.

It will be recalled that the greatest deviations between the generation and multigroup methods occurred for the calculation of the neutral density. The discrepancy will have a pronounced effect for a beam driven system such as TFTR. The probability of charge exchange of a hot beam ion is directly proportional to the background neutral density. The ensuing hot neutral, if it escapes from the

system, takes with it nearly all the energy of the original beam neutral. In the case of the ATC tokamak [24] calculations show that the surface energy loss due to this mechanism is an order of magnitude greater than that due to escaping background neutrals [25]. More importantly this represents ~ 50% of the original beam injected power and over 30% of the total input power. ATC plasma characteristics are not unlike those of the ST tokamak (e.g. a ~ 17 cm, $T_{imax} = 420$ eV for the beam injection phase). For a computer simulation of ATC therefore, a 30% overestimation of the beam charge exchange outflux due to an increased neutral population throughout the plasma (as implied from the results of Fig. 4(a)) would be significant.

Perhaps the most deleterious effects neutrals have on tokamak operation are the first wall sputtering damage caused by the fast charge exchange neutral outflux and the introduction of the sputtered impurities into the plasma. The fitted energy-dependent sputtering yield curve of Meade[26] is multiplied by the calculated neutral outflux to obtain the sputtering rates presented in Table XI. The neutrals are incident on a stainless steel vacuum wall located at the outer boundary. In general the multigroup sputtering rates are lower, with most of the difference accounted for by lower outflux levels.

An interesting trend is seen when the entries labeled Normal Incidence are compared with those labeled Angular Incidence. The former assume the sputtering yield is

independent of angle, and are calculated using Meade's normal incidence curve for all angles. However, the theory of Sigmund [27] predicts the sputtering yield should be approximately proportional to $1/\cos\theta$ where θ is the angle from the surface normal. (This theory is supported by measurements by Summer [28] of sputtering by 12 keV D+ on niobium.) When this angular dependence is included in the calculation, there are pronounced effects on sputtering rates. If the calculated angular distributions of neutrals at the wall were identical, a uniform increase would be expected. As it is, multigroup results increase by ~70% and ~115% for the ST and TFTR cases, respectively, while there are ~18% and ~61% increases given by the generation method. The effect is greater for the multigroup method because the $1/\cos\theta$ term increases the weights of neutrals with angles closer to a grazing incidence; these are present in greater proportion in the multigroup solution. This is because many neutrals originate from directions down the length of the cylinder and from volumes close to the surface (from first generation charge exchange) that are not considered explicitly in the 2-D disk geometry of the Düchs code. The angular sputtering effect is larger for the TFTR plasma than for the ST because the increased density and temperature leads to enhanced formation rates of charge exchange neutrals closer to the wall surface. Of final note is the increase in the sputtering rates, with or without the angular term, from the ST to TFTR machines. Although the

neutral outfluxes are comparable, the harder TFTR spectrum is distributed closer to the sputtering yield peak (~ 4 keV), which accounts for the order of magnitude difference.

6. CONCLUDING REMARKS

The multigroup method has been found to be an effective way of treating neutral atom transport in tokamak plasmas. The primary advantage of the multigroup method (over other neutral treatments) lies in the greater accuracy of the solutions that are obtained. We refer here to a fewer number of approximations and simplifications used in all aspects of the problem (e.g. cross section behavior, angular variations, problem convergence, geometry, etc.). In particular we demonstrate this to be true in the case of the widely used generation method.

To determine the practicality of utilizing the multigroup method as a neutral transport module (in a larger plasma code) we compared our results with those of the generation method. Test cases with significantly different plasma characteristics were chosen. Given the greater rigor of the multigroup method it is possible to check the accuracy of the generation treatment. In this regard we conclude that the generation method is sufficient to within a factor of three for the prediction of neutral densities. Parameters relating to the neutral outflux agree to within about 40% for the types of plasmas we have studied. We find

that these discrepancies may be of significance when a neutral transport module is used in conjunction with a plasma simulation code. We additionally observe that the multigroup results are more favorable for tokamak operation since the calculated neutral densities are lower, as are the charge exchange neutral outfluxes.

From the results of the comparison study, the disadvantage of the multigroup method appears to be in execution time. However, it was shown that a relaxation in operating parameters, with the inclusion of several supplementary time reduction techniques, could lower the multigroup run times by over two orders of magnitude to a level comparable to that of the generation method. For this case the multigroup results were additionally observed to be in better agreement with the neutral benchmark run. The multigroup method is therefore an attractive alternative for a transport module application. It is recalled that the generation method in its present form (a relatively quick procedure) requires more than 80% of the total Düchs code run time. To better this existing level with multigroup discrete ordinates methods for the general transport problem would be difficult. We have seen though that the reliability of the generation solution may be questionable for plasma configurations of future interest and so it may be advantageous to adopt a multigroup analysis or modify the present treatment. The replacement of the exponential attenuation factor by the K_{i1} function should benefit the generation method if the latter course is chosen. If this

is the case, multigroup discrete ordinates methods can continue to serve as a benchmark for the normalization of any such revised procedure.

ACKNOWLEDGMENT

This work is supported by the Energy Research and Development Administration Contract EY-76-C-02-3073.

The authors wish to thank Dr. D. E. Post for providing the results of the neutral transport calculations from the Düchs code.

REFERENCES

- [1] D. F. DÜCHS, D. E. POST, P. H. RUTHERFORD, Nuclear Fusion 17, 565 (1977).
- [2] G. I. BELL, S. GLASSTONE, Nuclear Reactor Theory (Van Nostrand Rheinhold Company, New York, 1970).
- [3] D. N. ZUBAREV, U. N. KLIMOV, Plasma Physics and the Problem of Controlled Thermonuclear Reactions, (Pergamon Press, New York, 1959) Vol. I., p. 162.
- [4] Y. N. DNESTROVSKII, D. P. KOSTOMAROV, N. L. PAVLOVA, Princeton Plasma Physics Laboratory Report Translation MATT-TRANS-107 (1971).
- [5] S. REHKER, H. WOBIG, Plasma Physics 15, 1083 (1973).
- [6] J. T. HOGAN, J. F. CLARKE, Surface Effects in Controlled Fusion, H. Wiedersich, M. S. Kaminsky, K. M. Zwilsky, eds. (North-Holland Publishing Company, Amsterdam, 1974) pp. 1-8.
- [7] J. F. CLARKE, D. J. SIGMAR, Proceedings of the Seventh European Conference on Controlled Fusion and Plasma Physics (Centre de Recherches en Physique des Plasmas, Lausanne, 1975) Vol. I., p. 134.

[8] K. MOLVIG, Massachusetts Institute of Technology, Research Laboratory of Electronics Report, April 1976.

[9] B. LEHNERT, Nuclear Fusion 8, 173 (1968).

[10] Handbook of Mathematical Functions, M. Abramowitz, I. A. Stegun, eds., (National Bureau of Standards, Washington, D. C., 1964) p. 483.

[11] E. GREENSPAN, Nuclear Fusion 14, 771 (1974).

[12] J. G. GILLIGAN, S. L. GRALNICK, W. G. PRICE, JR., Bull. Am. Phys. Soc. II 19, 853 (1974).

[13] J. H. MARABLE, E. M. OBLOW, Nuclear Science and Engineering 61, 90 (1976).

[14] Z. EL DERINI, E. M. GELBARD, Trans. Am. Nuc. Soc. 23, 45 (1976).

[15] B. G. CARLSON, K. D. LATHROP, Computing Methods in Reactor Physics, H. Greenspan, C. N. Kelber, D. Okrent, eds., (Gordon and Breach, New York, 1968) p. 171.

[16] K. D. LATHROP, Nuclear Science and Engineering 24, 381 (1966).

- [17] A. C. RIVIERE, *Nuclear Fusion* 11, 363 (1971).
- [18] M. T. ROBINSON, paper presented at 3rd National Conference, Atomic Collisions in Solids, Kiev, USSR, October 1974.
- [19] D. L. DIMOCK, H. P. EUBANK, E. HINNOV, L. C. JOHNSON, E. B. MESERVEY, *Nuclear Fusion* 13, 271 (1973).
- [20] Tokamak Fusion Test Reactor, Final Conceptual Design Report, Princeton Plasma Physics Laboratory Report PPPL-1275 (1976).
- [21] W. W. ENGLE, JR., A Users Manual for ANISN, Oak Ridge Gaseous Diffusion Plant Report K-1693 (1967).
- [22] W. STODIEK, K. BOL, H. EUBANK, S. VON GOELER, D. J. GROVE, Plasma Physics and Controlled Nuclear Fusion Research (International Atomic Energy Agency, Vienna, 1971) Vol. I, p. 465.
- [23] E. HINNOV, *Journal of Nuclear Materials* 53, 9 (1974).
- [24] K. BOL, et al., Plasma Physics and Controlled Nuclear Fusion Research (International Atomic Energy Agency, Vienna, 1975) Vol. I, p. 77.

[25] S. A. COHEN, Journal of Nuclear Materials 63, 65 (1976).

[26] D. M. MEADE, H. P. FURTH, P. H. RUTHERFORD, F. G. R. SEIDL, D. F. DÜCHS, Plasma Physics and Controlled Nuclear Fusion Research (International Atomic Energy Agency, Vienna, 1975) Vol. I., p. 605.

[27] P. SIGMUND, Phys. Rev. 89, 383 (1969).

[28] A. J. SUMMER, N. J. FREEMAN, N. R. DALY, J. Appl. Phys. 42, 4774 (1971).

[29] J. G. GILLIGAN, Ph.D. Dissertation, The University of Michigan (1977).

[30] J. G. GILLIGAN, S. L. GRALNICK, W. G. PRICE, JR., T. KAMMASH, Trans. Am. Nucl. Soc. 26, 87 (1977).

APPENDIX

To follow the approximations introduced by the Düchs generation method in treating the exact neutral transport problem we substitute equations (3) and (4) into equation (2) and solve iteratively for the angular neutral density of the next charge exchange "generation" (n^{g+1}) in dE about E and $d\Omega$ about Ω as

$$n^{g+1}(\underline{r}, \underline{\Omega}, E) dE d\Omega = \int_0^\infty ds' \exp \left[- \int_0^{s'} ds'' \left(\frac{N_i(\underline{r}-s''\underline{\Omega}) \langle \sigma v \rangle_{cx}(\underline{r}-s''\underline{\Omega}, E)}{v} + \frac{N_e(\underline{r}-s''\underline{\Omega}) \langle \sigma v \rangle_{ei}(\underline{r}-s''\underline{\Omega}, E)}{v} \right) \right] \quad (A1)$$

$$\times \frac{N_i(\underline{r}-s'\underline{\Omega})}{4\pi v} h_i(\underline{r}-s'\underline{\Omega}, E) \int_{E', \underline{\Omega}'} n^g(\underline{r}-s'\underline{\Omega}, \underline{\Omega}', E') |\underline{v}-\underline{v}'| \sigma_{cx}(|\underline{v}-\underline{v}'|) dE' d\Omega' dE d\Omega$$

where we have neglected ion impact ionization, (a good approximation for $E < 10$ keV), and have identified

$$\langle \sigma v \rangle_{cx}(\underline{r}, E) = \int_{E', \underline{\Omega}'} h_i(\underline{r}, E') |\underline{v}-\underline{v}'| \sigma_{cx}(|\underline{v}-\underline{v}'|) \frac{dE' d\Omega'}{4\pi} \quad (A2)$$

$$\langle \sigma v \rangle_{ei}(\underline{r}, E) = \int_{E', \underline{\Omega}'} h_e(\underline{r}, E') |\underline{v}-\underline{v}'| \sigma_{ei}(|\underline{v}-\underline{v}'|) \frac{dE' d\Omega'}{4\pi} \quad (A3)$$

The third line of equation (A1) represents the source of charge exchange neutrals for the $g+1$ generation. The source is a function of the angle $\underline{\Omega}$ because of the coupling between $\underline{\Omega}$ and $\underline{\Omega}'$ in the relative velocity $|\underline{v} - \underline{v}'|$ and the general angular dependence of $n^g(\underline{\Omega}')$ (the angular density of the current generation). A great deal of simplification can be realized, however, by effectively eliminating the dependence. There are several physical situations which may justify this assumption (not mentioned in Ref. [1]). The first has been noted before, namely, that the charge exchange cross section can be approximated as in equation (7). Alternatively, it can be assumed that the energies of the neutrals are either much greater than or much less than those of the target ions (which will occur in certain regions of the plasma). This permits the following:

$$|\underline{v} - \underline{v}'| \sigma_{cx}(|\underline{v} - \underline{v}'|) \sim v' \sigma_{cx}(v') \quad \text{for } v' \gg v$$

or

(A4)

$$|\underline{v} - \underline{v}'| \sigma_{cx}(|\underline{v} - \underline{v}'|) \sim v \sigma_{cx}(v) \quad \text{for } v \gg v'$$

A final possibility assumes that the angular density of the previous generation of neutrals is isotropic (independent of $\underline{\Omega}'$). This would be the case in an infinite homogeneous medium problem. Any of the assumptions allow the decoupling of the angular integral in the source function, which leads to an approximation for the new charge exchange source as

$$\begin{aligned} & \frac{N_i(\underline{r}-\underline{s}'\underline{\Omega})}{4\pi v} h_i(\underline{r}-\underline{s}'\underline{\Omega}, E) \int_{E', \underline{\Omega}'} n^g(\underline{r}-\underline{s}'\underline{\Omega}, \underline{\Omega}', E') |\underline{v}-\underline{v}'| \sigma_{CX}(|\underline{v}-\underline{v}'|) dE' d\underline{\Omega}' dE d\underline{\Omega} \\ & = \frac{N_i(\underline{r}-\underline{s}'\underline{\Omega})}{4\pi v} h_i(\underline{r}-\underline{s}'\underline{\Omega}, E) \int_{E'} n^g(\underline{r}-\underline{s}'\underline{\Omega}, E') \int_{\underline{\Omega}'} |\underline{v}-\underline{v}'| \sigma_{CX}(|\underline{v}-\underline{v}'|) \frac{d\underline{\Omega}' dE'}{4\pi} dE d\underline{\Omega} \end{aligned} \quad (A5)$$

where $n^g(\underline{r}-\underline{s}'\underline{\Omega}, E') = \int n^g(\underline{r}-\underline{s}'\underline{\Omega}, \underline{\Omega}', E') d\underline{\Omega}'$. The Düchs treatment additionally assumes that the just born neutrals are monoenergetic with a kinetic energy related to the local ion temperature at the point of creation. This specification implies that the ion distribution function is approximated as

$$h_i(\underline{r}-\underline{s}'\underline{\Omega}, E) = \delta(E - kT_i(\underline{r}-\underline{s}'\underline{\Omega})) \quad (A6)$$

The energy distribution of the current generation (n^g) is also specified, assumed monoenergetic and represented by

$$n^g(\underline{r}-\underline{s}'\underline{\Omega}, E') = n^g(\underline{r}-\underline{s}'\underline{\Omega}) \delta(E' - kT^g(\underline{r}-\underline{s}'\underline{\Omega})) \quad (A7)$$

The "temperature" at the radial position \underline{r} is given by averaging over the temperatures of the neutrals that reach the point \underline{r} . i.e.

$$T^{g+1}(\underline{r}) = \int T_i(\underline{r}-\underline{s}'\underline{\Omega}) dn^g(\underline{r}-\underline{s}'\underline{\Omega}) / n^{g+1}(\underline{r}) \quad (A8)$$

Equations (A5), (A6) and (A7) are substituted into equation (A1) and the integration over energy is performed to give

$$n^{g+1}(\underline{r}, \underline{\Omega}) d\underline{\Omega} = \int_0^{\infty} ds' d\underline{\Omega} \frac{N_i(\underline{r}-s'\underline{\Omega})}{4\pi v_i} n^g(\underline{r}-s'\underline{\Omega}) \langle \overline{\sigma v} \rangle_{cx}(\underline{r}-s'\underline{\Omega}) \quad (A9)$$

$$\times \exp \left[- \int_0^{s'} ds'' \left(\frac{N_i(\underline{r}-s''\underline{\Omega}) \langle \overline{\sigma v} \rangle_{cx}(T_i)}{v_i} + \frac{N_e(\underline{r}-s''\underline{\Omega}) \langle \overline{\sigma v} \rangle_{ei}(T_i)}{v_i} \right) \right]$$

where

$$\langle \overline{\sigma v} \rangle_{cx}(\underline{r}-s'\underline{\Omega}) = \int_{E', \underline{\Omega}'} \delta(E' - kT^g(\underline{r}-s'\underline{\Omega})) |\underline{v}_i - \underline{v}'| \sigma_{cx}(|\underline{v}_i - \underline{v}'|) dE' \frac{d\underline{\Omega}'}{4\pi} \quad (A10)$$

and

$$v_i(\underline{r}-s'\underline{\Omega}) = \left(\frac{2kT_i(\underline{r}-s'\underline{\Omega})}{m_i} \right)^{1/2} \quad (A11)$$

Attention is now brought to the evaluation of the angle integrals of equation (A9). Since the calculation will be carried out in infinite cylindrical geometry (one space dimension) the solid angle is given by

$$\int d\underline{\Omega} = \int_0^{2\pi} d\theta \int_{-1}^1 d\mu \quad (A12)$$

where

$$\cos \theta = \frac{\hat{\underline{\Omega}} \cdot \underline{r}}{|\underline{r}|} \quad \mu = \frac{\underline{\Omega} \cdot \underline{z}}{|\underline{z}|} = \cos \phi \quad (A13)$$

The orientation of the angles is shown in Fig. A.1. The unit vector $\hat{\underline{\Omega}}$ is assumed to lie in the x-y plane. When the integration over $\underline{\Omega}$ is performed for equation (A9), s' and s'' refer to line integrals along the direction $\underline{\Omega}$. The line

integrals can be simplified to in-plane distances (\hat{s}' and \hat{s}'' in the x-y plane of Fig. A.1(a)) by noticing that

$$ds' = \frac{d\hat{s}'}{\sqrt{1-\mu^2}} \quad (A14)$$

$$ds'' = \frac{d\hat{s}''}{\sqrt{1-\mu^2}}$$

Using equations (A14) and integrating over $\underline{\Omega}$, equation (A9) becomes

$$\begin{aligned} n^{g+1}(\underline{r}) &= \int_0^{2\pi} \int_{-1}^1 n^{g+1}(\underline{r}, \underline{\Omega}) d\mu d\theta \\ &= \int_0^{2\pi} \frac{d\theta}{4\pi} \int_{-1}^1 d\mu \int_{P'(\underline{r})}^{P(\underline{r}, \theta)} \frac{d\hat{s}'}{\sqrt{1-\mu^2}} \frac{N_i(\underline{r}-\hat{s}'\underline{\Omega})}{v_i} n^g(\underline{r}-\hat{s}'\underline{\Omega}) \langle \sigma \bar{v} \rangle_{cx}(\underline{r}-\hat{s}'\underline{\Omega}) \\ &\quad \times \exp \left[- \int_{P'(\hat{s}')}^{P''(\underline{r})} \frac{d\hat{s}''}{\sqrt{1-\mu^2}} \left(\frac{N_i(\underline{r}-\hat{s}''\underline{\Omega}) \langle \sigma \bar{v} \rangle_{cx}(T_i)}{v_i} + \frac{N_e(\underline{r}-\hat{s}''\underline{\Omega}) \langle \sigma \bar{v} \rangle_{ei}(T_i)}{v_i} \right) \right] \end{aligned} \quad (A15)$$

where the line integrals are now over \hat{s}' and \hat{s}'' and the limits are given in Fig. A.1. Since $n^g(\underline{r})$ is independent of μ , the integral over the variable μ may be brought out of equation (A15) to yield an integral of the form:

$$I(\hat{s}') = \int_{-1}^1 d\mu \frac{1}{\sqrt{1-\mu^2}} \exp \left[- \left[\frac{1}{\sqrt{1-\mu^2}} \rho(\hat{s}') \right] \right] \quad (A16)$$

where we have identified the optical depth as

$$\rho(\hat{s}') = \int_{P'(\hat{s}')}^{P''(\underline{r})} d\hat{s}'' \left(\frac{N_i(\underline{r}-\hat{s}''\hat{\Omega}) \langle \sigma v \rangle_{cx}(T_i)}{v_i} + \frac{N_e(\underline{r}-\hat{s}''\hat{\Omega}) \langle \sigma v \rangle_{ei}(T_i)}{v_i} \right) \quad (A17)$$

To perform the integral of equation (A16) we introduce the convenient change of variables

$$\mu = \tanh t \quad (A18)$$

which allows equation (A16) to be written as

$$I(\hat{s}') = 2 \int_0^{\infty} \frac{\exp[-\rho(\hat{s}') \cosh t]}{\cosh t} dt = 2 \text{Ki}_1(\rho) \quad (A19)$$

where Ki_1 is identified as the first repeated integral of the Bessel function [10].

With the results (A19), equation (A15) can be simplified to the form

$$n^{g+1}(\underline{r}) = \int_0^{\pi} \frac{d\theta}{\pi} \int_{P''(\underline{r})}^{P(\underline{r}, \theta)} \frac{N_i(\underline{r}-\hat{s}'\hat{\Omega})}{v_i} n^g(\underline{r}-\hat{s}'\hat{\Omega}) \langle \sigma v \rangle_{cx}(\underline{r}-\hat{s}'\hat{\Omega}) \text{Ki}_1(\rho(\hat{s}')) d\hat{s}' \quad (A20)$$

where we have used the fact that the solution will be symmetric about $\theta=\pi$.

The complicated dependence of Ki_1 on ρ can be approximated (to within 10%) by the exponential function in the range $.4 < \rho < 1$, as seen from Fig. A.2, which corresponds to the optical depth of many plasmas (e.g. for ST $\rho \sim .8$). However, most plasmas of future interest (PLT, TFTR, ALCATOR) have optical depths $\rho \geq 3$. For this range the exponential approximation is no longer valid. Notwithstanding this restriction, the exponential approximation allows equation (A20) to be reduced to

$$n^{g+1}(\underline{r}) = \int_0^\pi \frac{d\theta}{\pi} \int \frac{P(\underline{r}, \theta) N_i(\underline{r}-\hat{s}', \hat{\Omega})}{v_i} n^g(\underline{r}-\hat{s}', \hat{\Omega}) \langle \overline{\sigma v} \rangle_{cx}(\underline{r}-\hat{s}', \hat{\Omega}) e^{-\rho(\hat{s}')} d\hat{s}'. \quad (A21)$$

Equation (A21) is the approximation to the integral Boltzmann equation that is solved for the neutral atom distribution by the generation method.

	ST	TFTR
r_0 (cm)	14	85
T_0 (eV)	490	9950
T_B (eV)	10	50
α	2	2
N_0 (cm ⁻³)	2.7×10^{13}	4.0×10^{13}
N_B (cm ⁻³)	3.0×10^{12}	1.0×10^{13}
β	2	3

TABLE I. Parameters for the fits used to determine plasma densities and temperatures in equation (14).

# Groups	Total Relative Attenuation	Avg. Energy of Outflux (eV)	Iteration Time* (sec)
11	4.82×10^3	2185	16.08
31	5.29×10^3	1854	75.24
50	5.32×10^3	1836	113.88

*IBM 360/91

TABLE II. Comparison of Group Structure (TFTR Configuration P_0, S_8).

	ST	TFTR
Geometry	Infinite Cylinder	Infinite Cylinder
Minor Radius (cm)	14	85
Spatial Intervals	00	99
Temperature Zones	99	99
Plasma Temp. $T_e = T_i$ (eV) [On axis At edge	4.99×10^2 2.08×10^1	9.99×10^3 2.49×10^2
Plasma Density $N_e = N_i$ (cm ⁻³) [On axis At edge	3.00×10^{13} 3.56×10^{12}	4.99×10^{13} 1.12×10^{13}
Nominal Energy of Source Neutrals (eV)	3	3
Order of Scattering Expansion	0 (Isotropic)	0 (Isotropic)
Order of Angular Quadrature	8	8
Energy Groups	31	31

TABLE III. Summary of parameters for the discrete ordinates transport code ANISN used for the multigroup solution.

	ST	TFTR
Geometry	Planar Disk	Planar Disk
Minor Radius (cm)	14	85
Spatial Intervals	99	99
Temperature Zones	99	99
Plasma Temp. $T_e = T_i$ (eV)	<div style="display: flex; align-items: center;"> <div style="margin-right: 10px;">[</div> <div style="margin-right: 10px;">On axis</div> <div style="margin-right: 10px;">4.99 x 10²</div> </div> <div style="display: flex; align-items: center;"> <div style="margin-right: 10px;">[</div> <div style="margin-right: 10px;">At edge</div> <div style="margin-right: 10px;">2.08 x 10¹</div> </div>	<div style="display: flex; align-items: center;"> <div style="margin-right: 10px;">9.99 x 10³</div> </div> <div style="display: flex; align-items: center;"> <div style="margin-right: 10px;">2.49 x 10²</div> </div>
Plasma Density $N_e = N_i$ (cm ⁻³)	<div style="display: flex; align-items: center;"> <div style="margin-right: 10px;">[</div> <div style="margin-right: 10px;">On axis</div> <div style="margin-right: 10px;">3.00 x 10¹³</div> </div> <div style="display: flex; align-items: center;"> <div style="margin-right: 10px;">[</div> <div style="margin-right: 10px;">At edge</div> <div style="margin-right: 10px;">3.56 x 10¹²</div> </div>	<div style="display: flex; align-items: center;"> <div style="margin-right: 10px;">5.00 x 10¹³</div> </div> <div style="display: flex; align-items: center;"> <div style="margin-right: 10px;">1.12 x 10¹³</div> </div>
Nominal Energy of Source Neutrals	3	3
Charge Exchange Generations	10	10
Reporting Energies	10	10

TABLE IV. Summary of parameters for the neutral transport module of the Duchs code (Generation method).

Scattering Approximation	Relative Neutral Density Attenuation	Average Energy of Outflux (eV)	Iteration* Time (sec)
P ₀	5.29 x 10 ³	1854	75.24
P ₁	5.29 x 10 ³	1805	84.84
P ₃	5.26 x 10 ³	1805	143.58

TABLE V. Comparison of the Order of Scattering Approximation (TFTR Configuration, S₈, 31 Groups, *IBM 360/91).

		ST	TFTR
Neutral Density at Edge (cm^{-3})		1×10^{10}	1×10^{10}
Neutral Density on Axis (cm^{-3})	G	1.57×10^8	5.59×10^6
	M	1.10×10^8	1.93×10^6
Outflux of Charge Exchange Neutrals ($\text{cm}^{-2} - \text{sec}^{-1}$)	G	4.10×10^{15}	4.53×10^{15}
	M	3.12×10^{15}	3.25×10^{15}
Average Energy of Outflux (eV)	G	321	1879
	M	302	1865

TABLE VI. Summary of neutral results for the comparison study.

		ST	TFTR
Run	G	~ 6	~ 6
Time	*		
(sec)	M	~ 120	~ 170

*Iteration Loop.

TABLE VII. Comparison of Code Execution Times on the IBM 360/91.

	Relative Density Attenuation	Average Energy of Outflux (eV)	Outflux Current* ($\text{cm}^{-2} \text{sec}^{-1}$)	Sput. Rate* Normal Inc. ($\text{cm}^{-2} \text{sec}^{-1}$)	Outflux Power* (kW)	Execution Time† (sec)
Benchmark	5.17×10^3	1866	3.20×10^{15}	6.82×10^{12}	853	167.7
10 Plasma Zones	4.98×10^3	1906	3.21×10^{15}	6.87×10^{12}	875	97.9
Relaxed Operating Parameters	4.78×10^3	2255	3.27×10^{15}	7.71×10^{12}	1054	2.28
Line 3 with Restart and Limit = 1	4.71×10^3	2257	3.27×10^{15}	7.71×10^{12}	1053	1.14
Generation	1.79×10^3	1879	4.51×10^{15}	10.3×10^{12}	1212	~ 6

* Normalized to a neutral edge density of $1 \times 10^{10} \text{ cm}^{-3}$.

† IBM 360/91

TABLE VIII. Comparison of time reduction runs for the TFTR Plasma.

		ST	TFTR
Neutral Density at Edge (cm^{-3})		1.0×10^{10}	1.0×10^{10}
Power of Outfluxed Neutrals (kW)	G	11.89	1211
	M	8.461	864.4

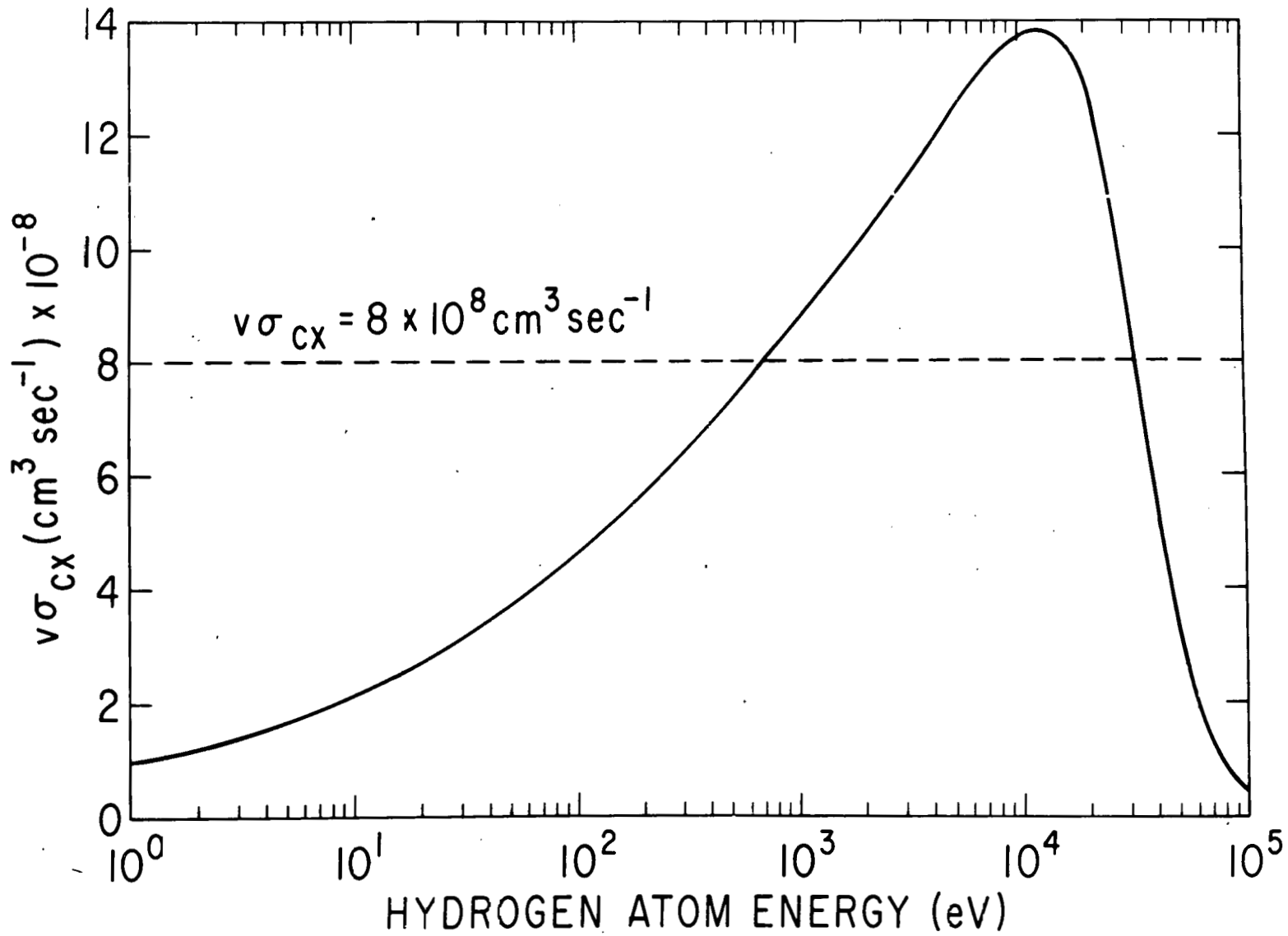
TABLE IX. The power of outfluxed charge change neutrals normalized to a neutral edge density of $1 \times 10^{10} \text{ cm}^{-3}$.

Hinnov (Experimental Observation)	Generation	Multigroup
70	69.6	64.9

TABLE X. Charge Exchange Power Loss for the ST Tokamak (kW), with each method normalized to an outflux level of $2.4 \times 10^{16} \text{ cm}^{-2} \text{ sec}^{-1}$.

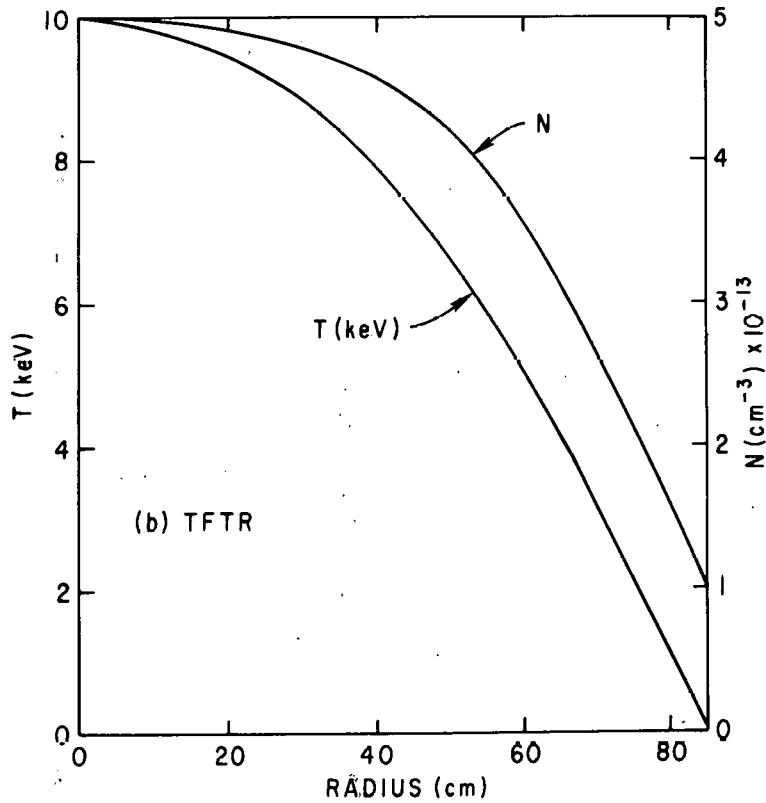
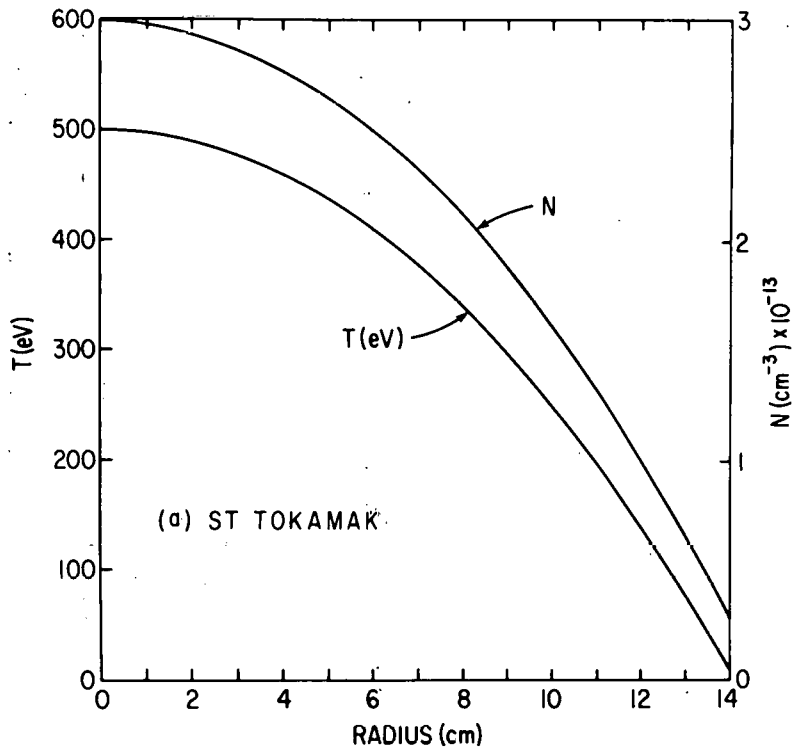
		ST	TFTR
Neutral Density at Edge (cm^{-3})		1.0×10^{10}	1.0×10^{10}
Total Sputtering Rate ($\text{cm}^{-2} - \text{sec}^{-1}$) Normal Incidence	G	1.47×10^{12}	1.04×10^{13}
	M	1.04×10^{12}	$.69 \times 10^{13}$
Total Sputtering Rate ($\text{cm}^{-2} - \text{sec}^{-1}$) Angular Incidence	G	1.73×10^{12}	1.67×10^{13}
	M	1.79×10^{12}	1.49×10^{13}

TABLE XI. The total sputtering rates for neutrals incident on a stainless steel vacuum wall.



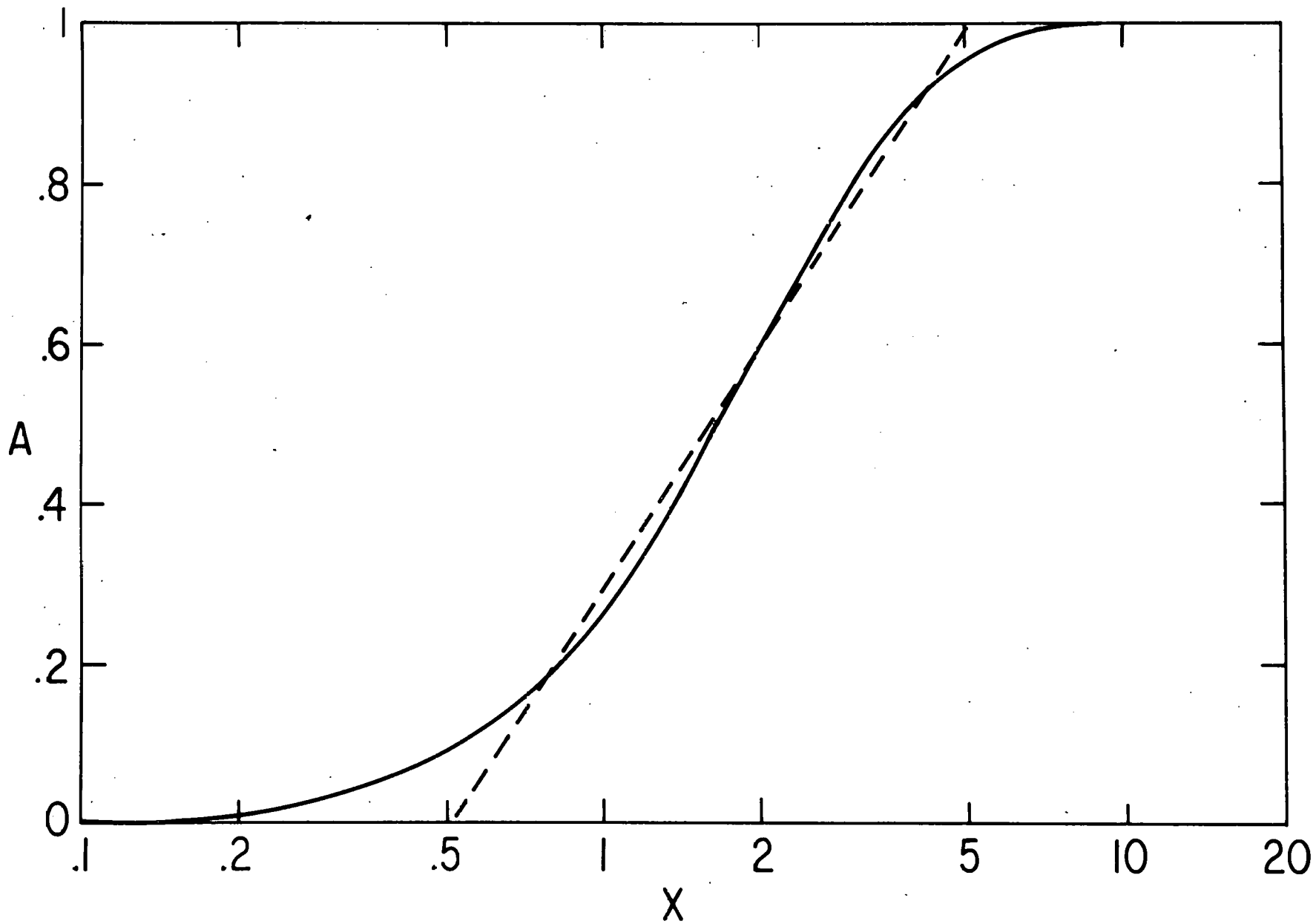
774101

Fig. 1. The charge exchange reaction rate ($v\sigma_{cx} \text{cm}^3 \text{sec}^{-1}$) vs. hydrogen atom energy.



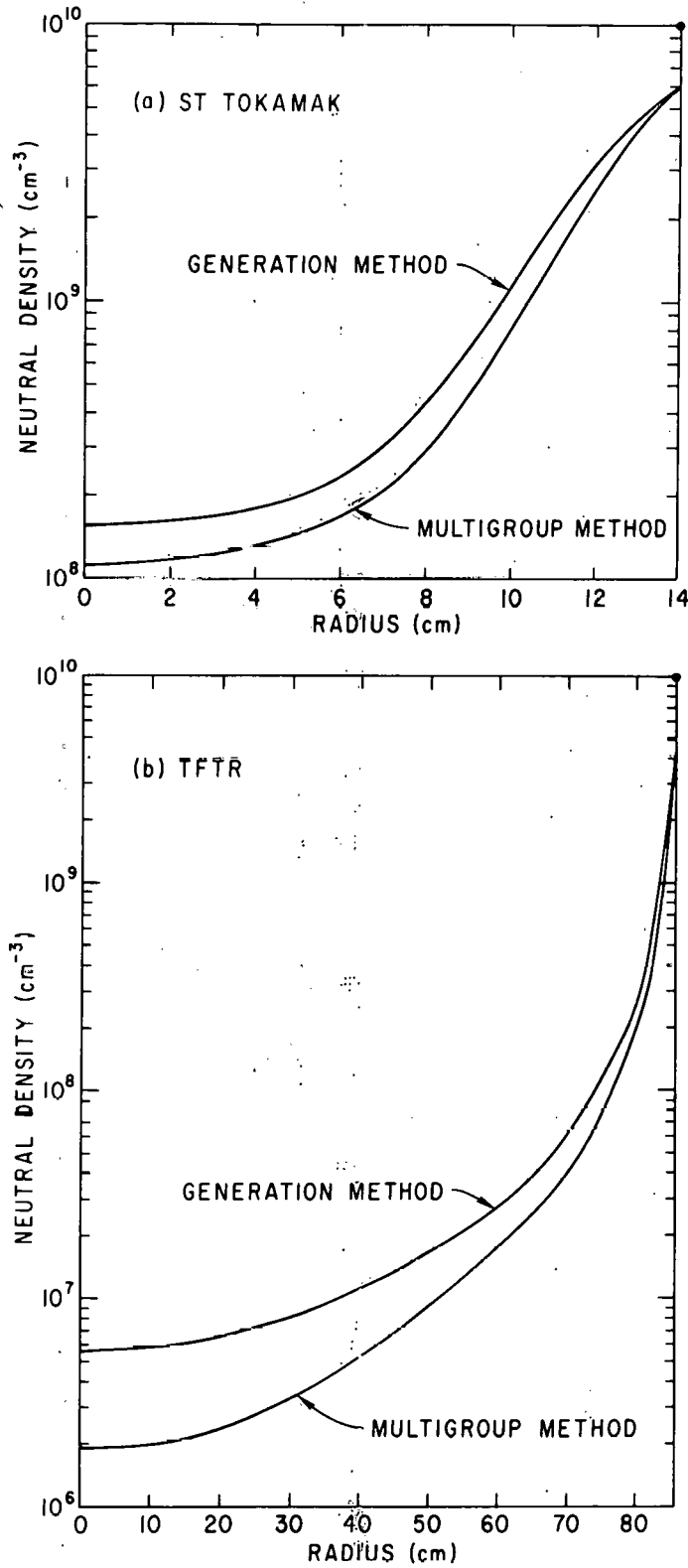
774104

Fig. 2. Plasma temperature ($T = T_i = T_e$) and density ($N = N_i = N_e$) profiles for the (a) ST and (b) TFTR Tokamaks.



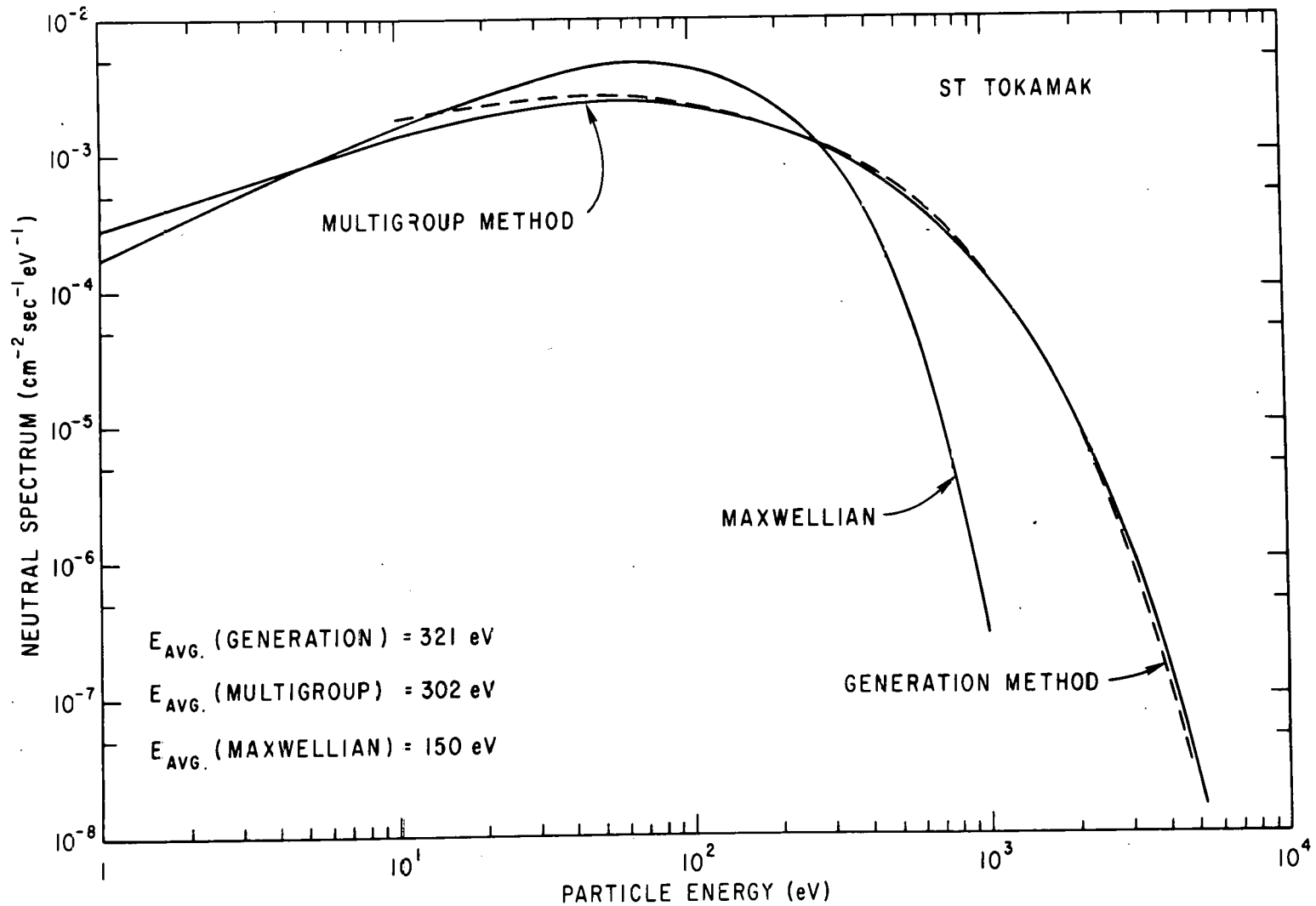
774659

Fig. 3. Semi-logarithmic plot of the fraction of total particles in a Maxwellian flux distribution (A) up to the normalized energy x .



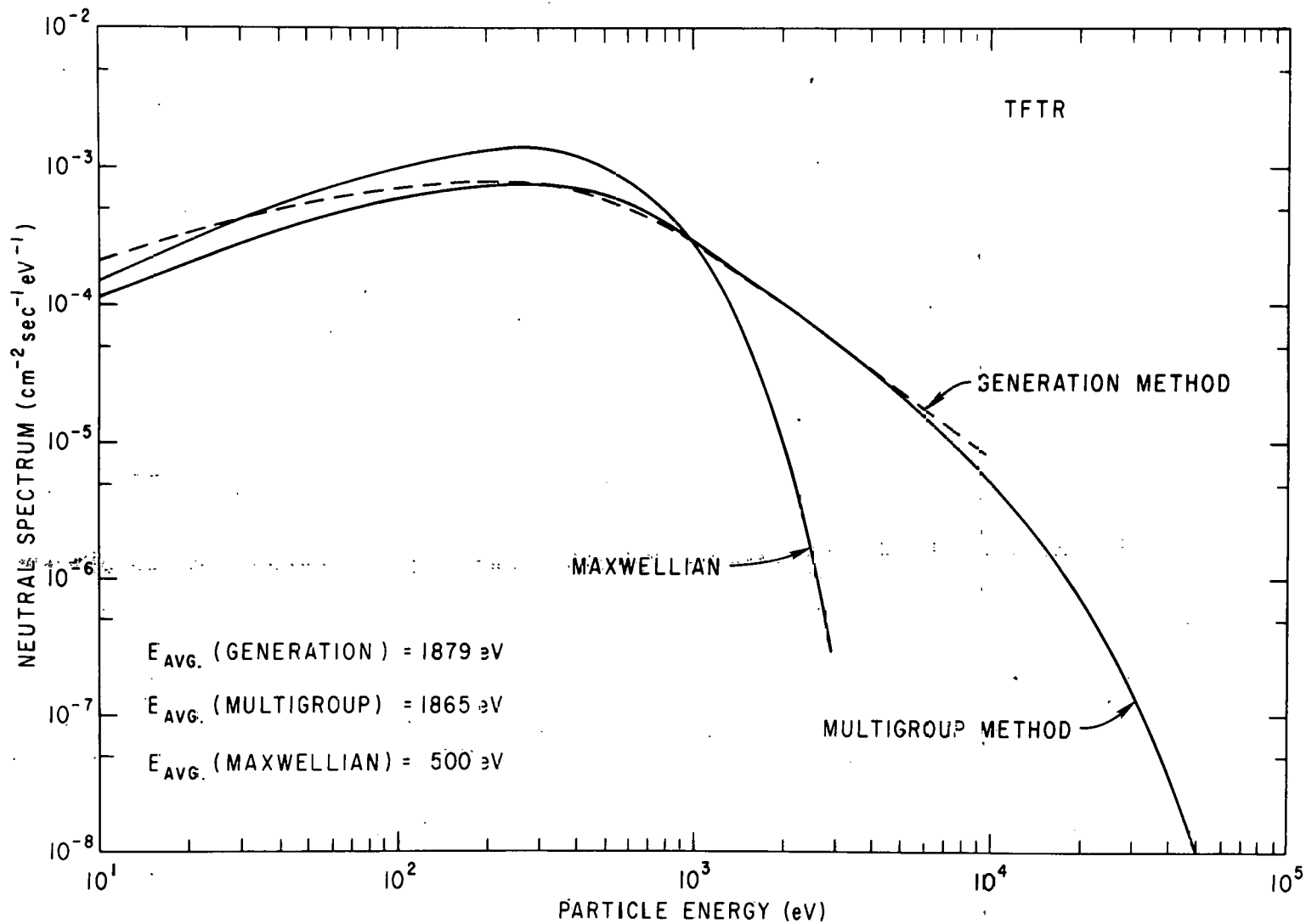
774105

Fig. 4. Calculated hydrogen atom densities for the (a) ST and (b) TFTR tokamaks vs. distance from the cylindrical axis. The results are normalized to a neutral edge density of $1 \times 10^{10} \text{ cm}^{-3}$.



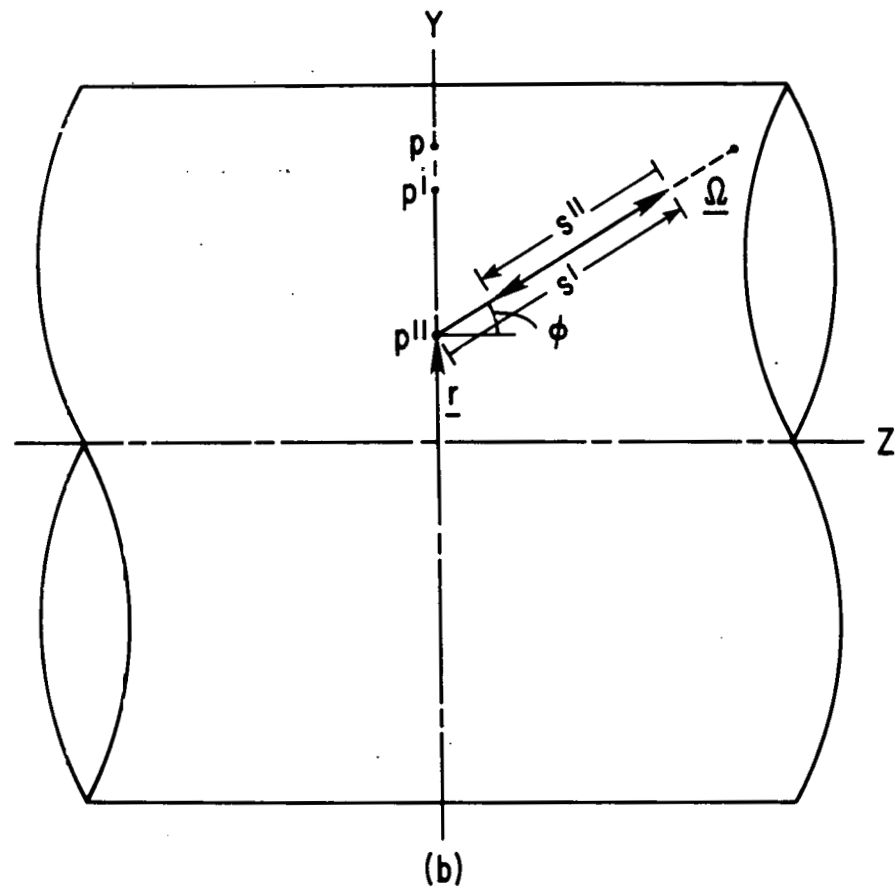
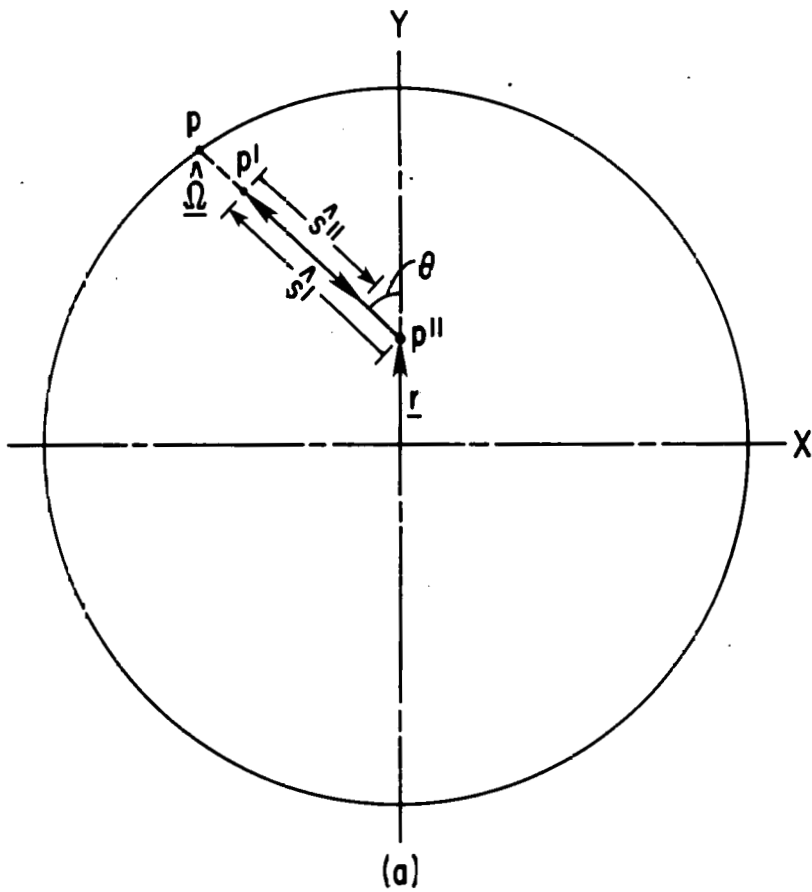
774103

Fig. 5. The spectrum of outfluxed charge exchange neutrals at the outer boundary ($r = 14 \text{ cm}$) of the ST tokamak vs. hydrogen atom energy. The total outflux is normalized to unity.



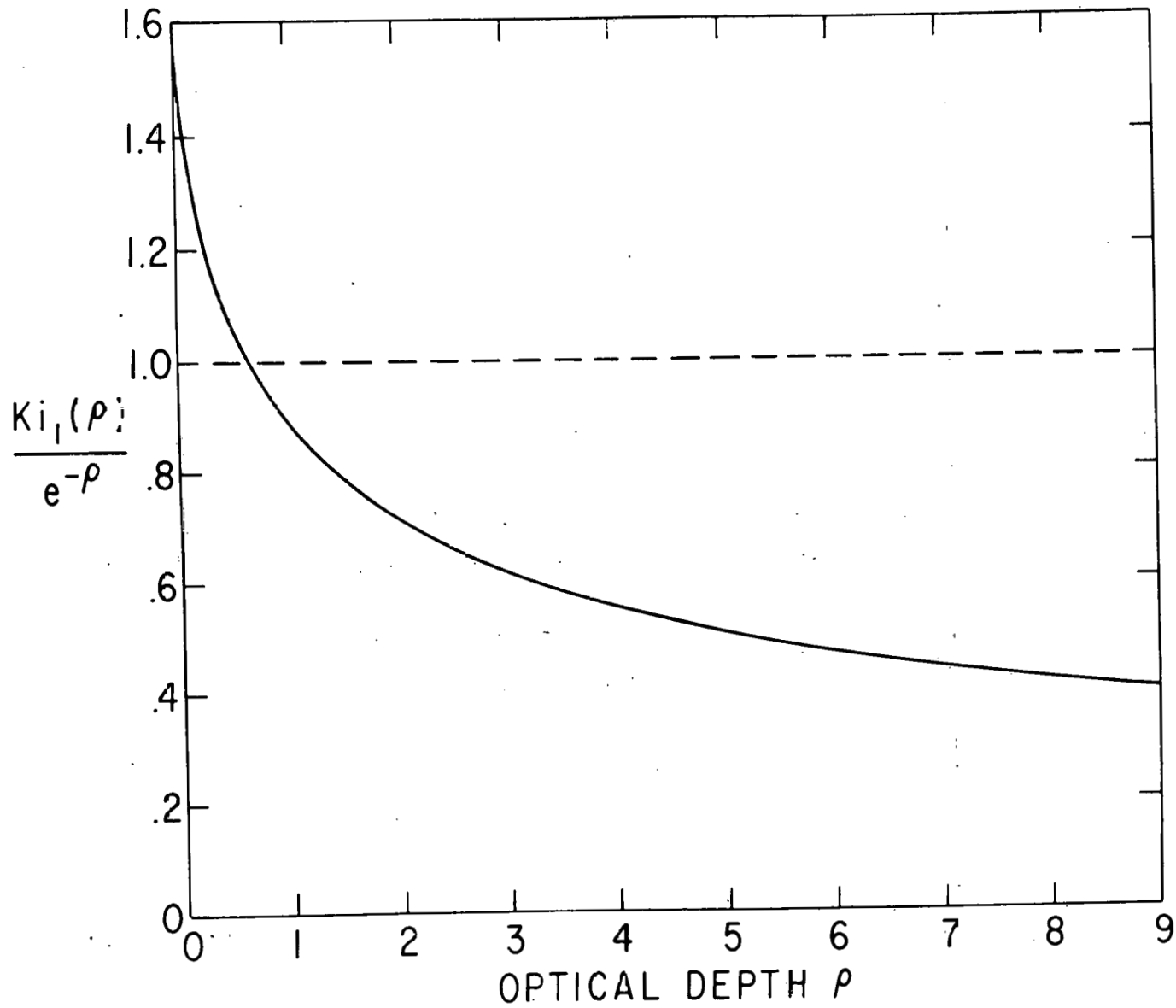
774102

Fig. 6. The spectrum of outfluxed charge exchange neutrals at the outer boundary ($r = 85 \text{ cm}$) of the TFTR tokamak vs. hydrogen atom energy. The total outflux is normalized to unity.



774099

Fig. A.1. Orientation of vectors for the integration of equation (A15) in infinite cylindrical geometry. The vectors in (a) lie in the x - y plane. In (b) the x axis is into the paper.



774100

Fig. A.2. The ratio of the First Repeated Integral of the Bessel Function (Ki_1) to the Exponential Function ($e^{-\rho}$) for values of the argument.